JGR Space Physics

RESEARCH ARTICLE
10.1029/2019JA026611

Key Points:
- Airglow patches detected using the Resolute Bay imager correspond to lobe structures discovered in Cluster spacecraft observations
- Lobe structures over patches contain locally enhanced flows, R-1 sense field-aligned currents, and field-aligned soft electron flux enhancements
- The lobe structures are driven by the magnetosphere, likely due to enhanced localized dayside reconnection and subsequent poleward propagation

Supporting Information:
- Supporting Information S1
- Movie S1
- Movie S2
- Movie S3

Correspondence to:
L. V. Goodwin,
lindsaygoodw@gmail.com

Citation:
Goodwin, L. V., Nishimura, Y., Zou, Y., Shiokawa, K., & Jayachandran, P. T. (2019). Mesoscale convection structures associated with airglow patches characterized using Cluster-imager conjunctions. *Journal of Geophysical Research: Space Physics*, *124*, 7513–7532. https://doi.org/10.1029/2019JA026611

Received 13 FEB 2019
Accepted 7 AUG 2019
Accepted article online 2 SEP 2019
Published online 11 SEP 2019

Mesoscale Convection Structures Associated With Airglow Patches Characterized Using Cluster-Imager Conjunctions

L. V. Goodwin[1], Y. Nishimura[2,3], Y. Zou[1,4], K. Shiokawa[5], and P. T. Jayachandran[6]

[1]Center for Space Physics and Department of Astronomy, Boston University, Boston, MA, USA, [2]Center for Space Physics and Department of Electrical and Computer Engineering, Boston University, Boston, MA, USA, [3]Department of Atmospheric and Oceanic Sciences, University of California, Los Angeles, CA, USA, [4]Cooperative Programs for the Advancement of Earth System Science, University Corporation for Atmospheric Research, Boulder, CO, USA, [5]Institute for Space-Earth Environmental Research, Nagoya University, Nagoya, Japan, [6]Physics Department, University of New Brunswick, Fredericton, New Brunswick, Canada

Abstract Polar cap ionospheric plasma flow studies often focus on large-scale averaged properties and neglect the mesoscale component. However, recent studies have shown that mesoscale flows are often found to be collocated with airglow patches. These mesoscale flows are typically a few hundred meters per second faster than the large-scale background and are associated with major auroral intensifications when they reach the poleward boundary of the nightside auroral oval. Patches often also contain ionospheric signatures of enhanced field-aligned currents and localized electron flux enhancements, indicating that patches are associated with magnetosphere-ionosphere coupling on open field lines. However, magnetospheric measurements of this coupling are lacking, and it has not been understood what the magnetospheric signatures of patches on open field lines are. The work presented here explores the magnetospheric counterpart of patches and the role these structures have in plasma transport across the open field-line region in the magnetosphere. Using red-line emission measurements from the Resolute Bay Optical Mesosphere Thermosphere Imager, and magnetospheric measurements made by the Cluster spacecraft, conjugate events from 2005 to 2009 show that lobe measurements on field lines connected to patches display (1) electric field enhancements, (2) Region 1 sense field-aligned currents, (3) field-aligned enhancements in soft electron flux, (4) downward Poynting fluxes, and (5) in some cases enhancements in ion flux, including ion outflows. These observations indicate that patches highlight a localized fast flow channel system that is driven by the magnetosphere and propagates from the dayside to the nightside, most likely being initiated by enhanced localized dayside reconnection.

1. Introduction

Dayside merging of the solar wind with the Earth's magnetosphere drives the Earth's magnetospheric generator and establishes perpendicular electric fields, creating the ionospheric convection streams observed in the polar cap (Dungey, 1961). Statistical studies of ionospheric convection have shown that during a southward interplanetary magnetic field (IMF), $-B_z$, the average high-latitude plasma convection pattern is overall characterized by a simple two-cell pattern, in which plasma structures in the polar cap move antisunward in association with the duskward convection electric field ($+E_y$). A dawnward motion ($-E_x$) then results under a negative IMF B_y, and a duskward motion ($+E_x$) results under a positive IMF B_y (Heelis, 1984; Heelis et al., 1982; Ruohoniemi & Greenwald, 1996; Weimer, 1995). Although large-scale statistical studies are useful for understanding the overall motion of plasma in the high-latitude ionosphere, they typically neglect smaller mesoscale flow structures, such as those collocated with enhanced density structures. Of particular interest to this work are airglow patches (or simply "patches"), which are 100- to 1,000-km-scale red-line emission structures in the *F* region polar cap, that are associated with polar cap patches (strictly speaking, plasma density enhancements at least twice that of the background plasma density). Patches are typically generated near the dayside cusp (e.g., Prikryl et al., 1999) from either (1) particle impact ionization (e.g., Goodwin et al., 2015; Kelley et al., 1982; MacDougall & Jayachandran, 2007; Moen et al., 2012; Walker et al., 1999; Weber et al., 1984) or (2) high-density dayside plasma becoming entrained in the polar cap (e.g., Carlson et al., 2004; Foster, 1984; Foster et al., 2005; Lockwood & Carlson, 1992; Lockwood et al., 2005;

Moen et al., 2006). In either case, once a patch is formed, it is transported along the streamlines of convection, and as they travel, plasma irregularities and scintillation effects form (e.g., Basu et al., 1990, 1994; Buchau et al., 1985).

An early study by Kivanç and Heelis (1997) explores small-scale flow structures (on the order of 500 m) associated with polar cap patches in the context of plasma density perturbations, showing that although the correlation between $\Delta N/N$ (where N is the plasma density) and an enhanced flow is weak, for a given intensity change in flow, $\Delta N/N$ maximizes in regions of large ΔN. Zou et al. (2015) present the results of a statistical study of polar cap flows associated with patches, showing that ~67% of airglow patches contain 200- to 300-km-wide enhanced antisunward flows, a few hundred meters per second larger than the background convection speed. Meanwhile, Zou et al. (2016) highlight the association among airglow patches, fast flow channels, and localized field-aligned currents (FACs), while Zou et al. (2017) show the collocation of enhanced electron fluxes (both structured and diffuse) with patches and mesoscale flows. A study by Zhang et al. (2017) has found flow channels to be particularly associated with polar cap patches that have relatively high electron temperatures, also known as "hot patches." These polar cap patches are also associated with enhanced particle precipitations, FACs, and ion upflows. Zhang et al. (2017) suggests that since hot polar cap patches can have the same order of density enhancement as classical polar cap patches, they may be produced by dayside photoionized plasma being transported into polar cap flow channels. Statistical results from Ma et al. (2018) indicate that hot polar cap patches have higher convection speeds and stronger FACs, while the classical polar cap patches in the central polar cap generally show lower convection speeds and weaker FACs. Their work suggests that hot polar cap patches are associated with the initial creation phase of polar cap patches and are associated with particle precipitation and bursty plasma flow, while the classical polar cap patches are more mature.

These studies compliment an earlier study by Nishimura et al. (2014) that tracks the evolution of a poleward moving auroral form, which are known to be connected with localized dayside magnetic merging events (Carlson et al., 2006; McWilliams et al., 2000; Sandholt et al., 2003). This poleward moving auroral form is associated with a flow channel (similar to Oksavik et al., 2004, or Oksavik et al., 2005) and evolves into an airglow patch that collides with the nightside auroral oval, resulting in a poleward boundary intensification. This observation underlines the importance of patches and mesoscale flows in coupling dayside merging with nightside reconnection across the polar cap. Additionally, this result is consistent with Lyons et al. (2011) and Nishimura et al. (2013), who both show poleward boundary intensifications resulting from enhanced flows impacting the nightside auroral oval and indicate the connection between patches and magnetospheric processes on the nightside.

Several of the aforementioned studies rather thoroughly characterize magnetosphere-ionosphere (MI) coupling through patches using ionospheric observations and contradict the notion that patches are simply localized regions of enhanced plasma that follow large-scale convection. However, these works are limited to the ionosphere, while magnetospheric studies related to polar cap patches have been very limited. Magnetohydrodynamic simulations by Nishimura and Lyons (2016) infer the existence of lobe convection structures and enhanced electric fields on open lobe field lines that map to mesoscale flows within the ionosphere. Nishimura and Lyons (2016) also indicate that these flow channels will drive faster plasma sheet thinning and localized magnetotail reconnection on the nightside. What remains unclear is whether we can observationally demonstrate the existence of magnetospheric structures corresponding to airglow patches, or whether the flow channels in the polar cap ionosphere are confined to the ionosphere. If they exist in the magnetosphere, it is then important to understand their properties and energy source, as well as their role in plasma transport and day-night reconnection coupling across the lobe and into the magnetotail. Since magnetospheric observations of patches have been severely lacking, it is difficult to examine whether active MI coupling exists over patches and, if so, to determine what drives the MI coupling. Motivated by this, the research presented here characterizes the lobe structures that correspond to patches. Works such as Vaith et al. (2004) have shown the usefulness of the Cluster spacecraft constellation in examining small-scale structures, such as electric field fluctuations superimposed on the average behavior of the high-latitude convection pattern. Therefore, the Cluster spacecraft are an ideal set of instruments with which to probe the lobe structures associated with airglow patches for the present study. Similar works have been performed by Lockwood, Opgenoorth, et al. (2001); Wild et al. (2001); and Lockwood, Fazakerley, et al. (2001), in which Cluster observations were coupled with such ground-based instrumentation as the European Incoherent Scatter Scientific Association (EISCAT) Svalbard Radar (ESR), the Collaborative UK Twin Located Auroral

Sounding System (CUTLASS), or the Super Dual Auroral Radar Network (SuperDARN). However, these studies predominately focused on flux transfer events and reconnection, or, in the case of Lockwood, Opgenoorth, et al. (2001), the electron flux of polar cap patches in relation to dayside merging. Therefore, this research focuses on electric field, magnetic field, and particle flux measurements from three of the Cluster spacecraft as their satellite footprints pass through airglow patches, which is inferred by red-line Resolute Bay images.

The Resolute Bay imager and the Cluster spacecraft are described in section 2, along with the process by which patches and spacecraft conjunctions are identified. Section 3 highlights the key results of this work, presenting both case studies and epoch studies of the magnetospheric structures associated with patches. Section 3 then briefly discusses how these observations show that the lobe structures associated with patches cannot be the result of either a neutral wind dynamo or a gradient drift instability (GDI) dynamo but are likely driven by the magnetosphere. Finally, section 4 summarizes the findings of this research.

2. Instrumentation and Methodology

Before the results of this work are presented, it is worthwhile briefly describing the instruments being used for this research. This section first states relevant information regarding the Resolute Bay red-line imager, after which key information about the Cluster spacecraft is presented.

2.1. Resolute Bay Imager

Utilizing data from the Resolute Bay Optical Mesosphere Thermosphere Imagers located at 74.73° N, 265.07° E (Hosokawa et al., 2006; Shiokawa et al., 1999, 2009), this research identifies airglow patches through the red-line (630.0 nm) airglow emissions that result from the de-excitation of oxygen atoms following the recombination of electrons and molecular oxygen ions. The imager obtains an all-sky image every 2 min during dark periods (~22 to ~15 Universal Time, UT, from September to March) using a 30-s exposure time. The readout noise and the dark noise of the charge-coupled device detector are 10 counts (root mean square) and far less than 1 (counts per pixel per second), respectively, making airglow emissions easily discernible from camera noise (Shiokawa et al., 1999). Given that red-line emissions occur between approximately 200- to 300-km altitude, imager data are mapped to an altitude of 250 km to identify patches.

Analogous to Hosokawa et al. (2009), this work defines airglow patches to be luminosity structures 5 R above the background luminosity with a peak luminosity above 10 R. The background is taken to be the minimum luminosity within 10 min of the suspected patch luminosity enhancement. Coincident green-line observations are also incorporated to differentiate patches from other luminosity structures, such as polar cap arcs. As has been done previously (Zou et al., 2016), as long as there are no substantial coincident green-line (557.7 nm) observations (5 R above the background luminosity with a peak luminosity above 10 R), the luminosity structure is considered a patch. In this work, the red-line emission within the patch is typically 10 times larger than the green-line intensity.

In addition to comparing red-line and green-line emissions, the work presented here compares red-line airglow emissions to Canadian Advanced Digital Ionosonde (CADI) measurements (Jayachandran et al., 2009). These instruments send a radio signal and record the received power for a range of plasma frequencies, which allows us to infer the plasma density from

$$\omega_{pe} = \sqrt{\frac{n_e e^2}{m_e \epsilon_0}}, \tag{1}$$

where ω_{pe} is the plasma frequency, n_e is the plasma/electron density, e is the elementary charge, m_e is the electron mass, and ϵ_0 is the permittivity of free space. This study utilizes both the Eureka ionosonde located at 88.10° N, 329.86° E and the Resolute bay ionosonde located at 83.13° N, 320.61° E (geomagnetic latitude and longitude).

2.2. Cluster

Cluster is a constellation of four polar-orbiting satellites organized in a tetrahedral configuration, orbiting the Earth every 57 hr with an apogee of 20 Earth radii and a perigee of 4 Earth radii. Each satellite contains identical instruments to resolve a variety of plasma parameters. The Electron Drift Instrument (EDI) is used to obtain electric field measurements at a resolution of 4 s (Paschmann et al., 2001). When EDI observations are unavailable, E_y is found using the Electric Field and Wave (EFW) experiment instrument (Gustafsson et al., 2001). EFW also provides the spacecraft potential data at a resolution of approximately 0.2 s and E_y at

a resolution of 4 s. The Fluxgate Magnetometer is used to determine the magnetic field at a resolution of 4 s (Balogh et al., 2001), as well as the FAC using Ampere's law:

$$J_{FAC} = \frac{(\nabla \times \delta B)_{||}}{\mu_0}, \tag{2}$$

where δB is a magnetic field perturbation relative to the T01 magnetic field model (Tsyganenko, 2002a, 2002b) and μ_0 is the vacuum permeability. We use the sheet current assumption to compute this equation from the Fluxgate Magnetometer measurements (Fukunishi et al., 1991), and we validate this assumption by comparing two successive satellite measurements. Given that the distance between the Cluster spacecraft is approximately the size of an airglow patch, the curlometer technique cannot be applied, making the sheet current assumption ideal. Using both the magnetic field and the electric field, **E**, it is possible to infer the direction of the Poynting vector, **S**, given by

$$\mathbf{S} = \frac{1}{\mu_0}\mathbf{E} \times \mathbf{B}. \tag{3}$$

Of final interest to this work is the three-dimensional distribution of magnetospheric ions resolved from the Cluster Ion Spectrometry (CIS) sensors with a resolution of 4 s (resampled using a 12-s median filter; Reme et al., 2001), and the three-dimensional distribution of electrons resolved from the Plasma Electron And Current Experiment (PEACE) sensors with a resolution of 4 s (Szita et al., 2001). It should be mentioned that measurements from the PEACE sensors are also able to validate when the Cluster spacecraft are traveling in the lobe, given that the lobe has a background energy typically between 10 and 100 eV (Pedersen et al., 2008). However, note that data from the Cluster 2 satellite are not available and that both the EDI and the Cluster Ion Spectrometry sensors on Cluster 4 are not operating. Thus, Cluster 1 and Cluster 3 are primarily used in this study.

The launch inclination of the four Cluster satellites was 90°, and from 2005 (when the Resolute Bay imager became operational) to 2009 (when the Cluster spacecraft began to probe lower latitudes), the Cluster spacecraft somewhat frequently traveled through the open field lines that mapped into the Resolute Bay imager field of view (FOV). These conjunctions are identified using the T01 magnetic field model, and conjunctions in which airglow patches are present are studied. This work identifies 38 satellite passes through airglow patches from 2005 to 2009. It is worth mentioning that the mapping locations do not change significantly when the T89, the T96, or the T04s magnetic field model is used (Tsyganenko, 1989, 1995; Tsyganenko & Sitnov, 2007), indicating that we can be confident in the accuracy of the field-line mapping performed. Additionally, the Cluster spacecraft are typically between three to seven Earth radii during the events of interest, where the magnetic field lines are reasonably dipolar and simpler to map into the ionosphere.

3. Results

Using the methodology described in the previous section, three cases are presented first to show the lobe structures that correspond to airglow patches in individual events. Results of the superposed epoch analysis based on the conjunctions from 2005 to 2009 are described next. Lastly, these results are discussed in the context of what drives the magnetospheric and ionospheric structures collocated with patches.

3.1. Case Studies

Before showing epoch studies of the structures that correspond to airglow patches, it is worthwhile exploring a few clear case studies of patches. Here, three case studies are presented. Case 1 shows a patch with clear lobe structures, while Case 2 shows a patch with similar lobe features but more substructures. Lastly, Case 3 shows one patch with no clearly associated lobe structures.

3.1.1. Case Study 1: 1 February 2006

Figure 1 shows Resolute Bay red-line imager data along with the corresponding IMF conditions on 1 February 2006. An airglow patch is located near the magnetic pole with a prenoon-premidnight orientation. The bright emission on the left side of the image is the duskside auroral oval. The motion of the patch is primarily antisunward, which is consistent with the predominately southward IMF. The patch also has a changing dawnward and then duskward motion, as is seen more clearly in Movie S1 in the supporting information. This is expected given the IMF reversal in B_y (Reiff & Burch, 1985). Figure S1 shows plasma frequency measurements from the Eureka ionosonde. The peak plasma frequency at 400 km changes from 5 MHz at 6:10 UT, when the ionosonde observes the patch of interest, to 3.5 MHz at 7:10 UT, when the

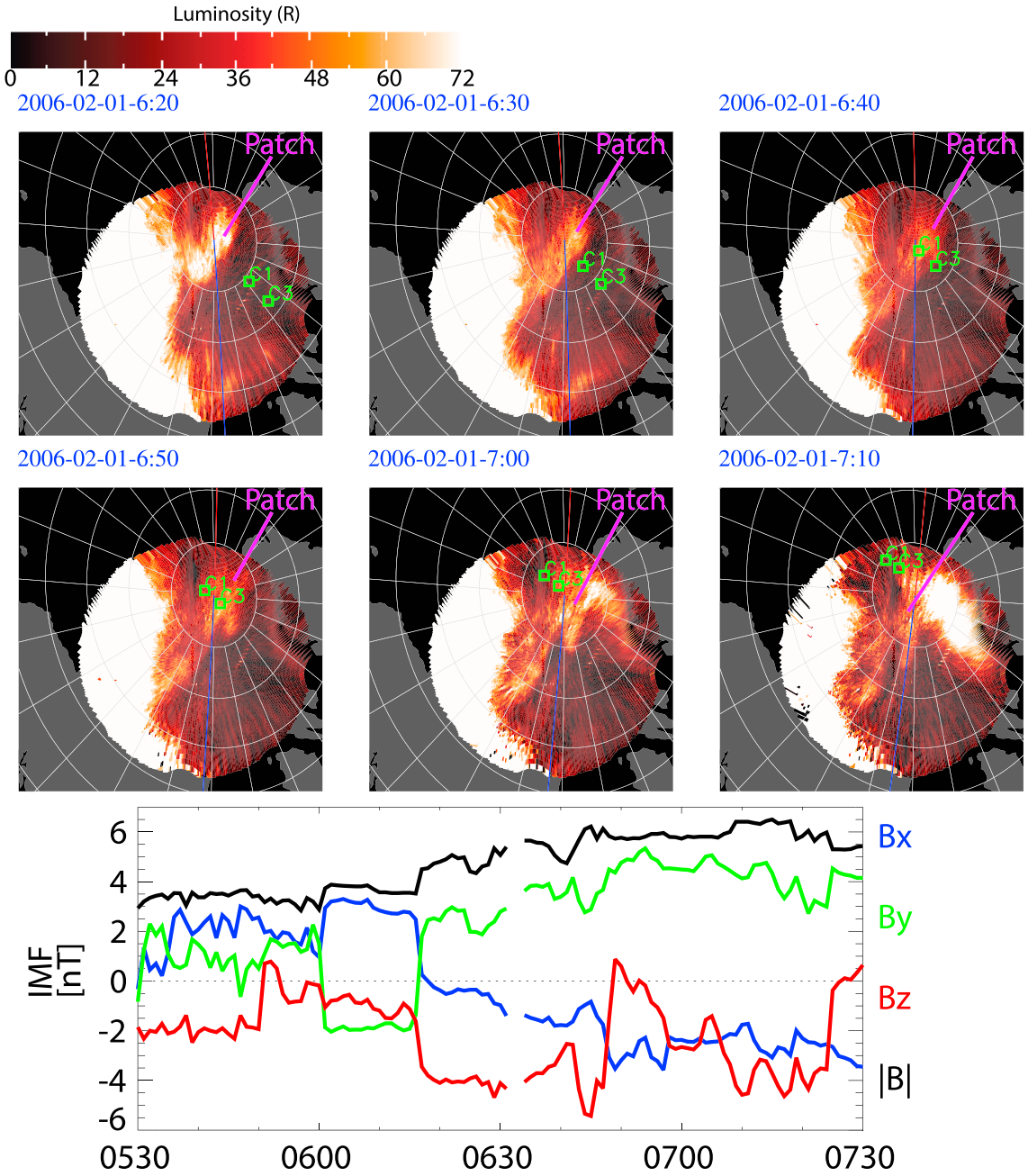

Figure 1. Red-line emission data from the Resolute Bay Optical Mesosphere Thermosphere Imagers instrument, along with the corresponding interplanetary magnetic field (IMF) conditions, for a 1 February 2006 airglow patch observation. The overlaid coordinates are altitude-adjusted corrected geomagnetic coordinates (given at 5° intervals in latitude and 1 hr in MLT), the red line indicates the direction of magnetic noon, the blue line indicates the direction of magnetic midnight, and the green squares indicate the Cluster spacecraft footprints. The line indicates the approximate patch location.

ionosonde observes the background polar cap. Given equation (1), this indicates that the density of the airglow structure observed in the imager data compared to the background changes by a factor of 2.3 and thus satisfies the definition of a polar cap patch (Crowley, 1996). Figure S2 presents Resolute Bay ionosonde observations in a similar format as Figure S1. Although the observations in Figure S2 are noisier (e.g., the vertical streaks are not associated with ionospheric plasma readings), the plasma frequency at 400 km changes from 4.5 MHz at 6:40 UT, when the ionosonde observes the patch of interest, to 3 MHz at 7:00 UT, when the ionosonde observes the background polar cap. The density enhancement observed by the Resolute Bay ionosonde is similar to that viewed by the Eureka ionosonde but is observed at a later time. This is consistent with the antisunward airglow patch motion observed in Movie S1.

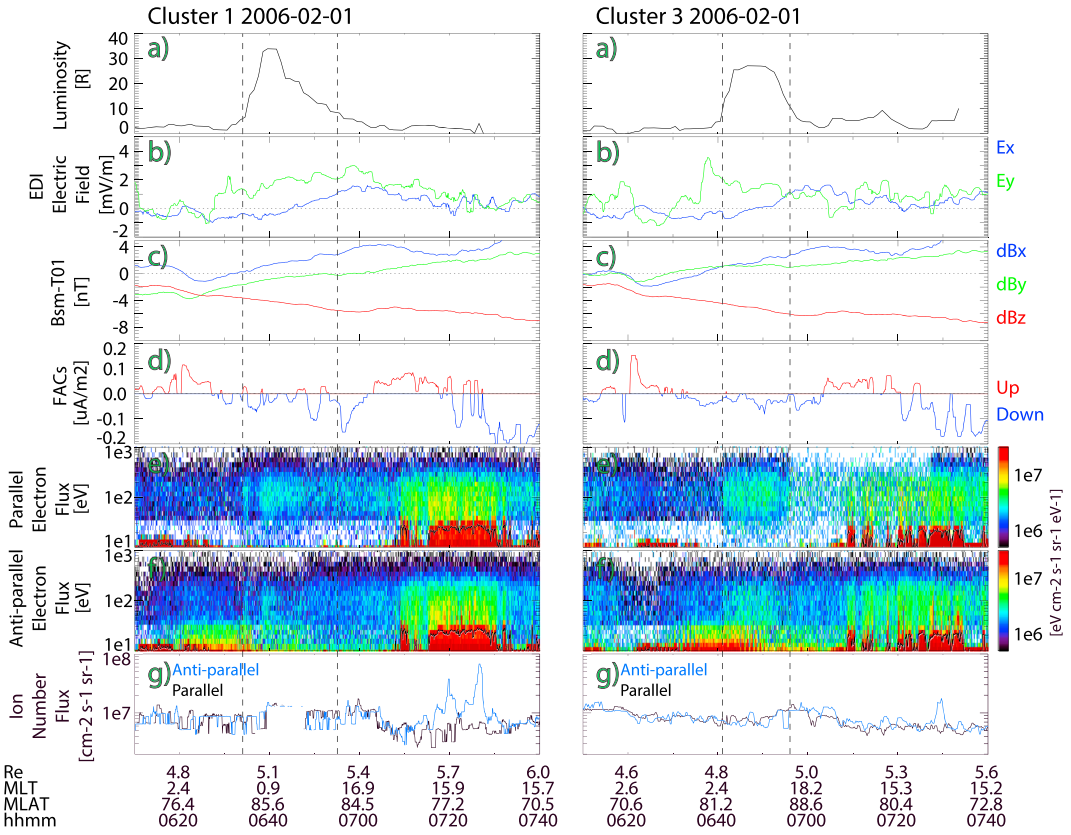

Figure 2. Cluster 1 (left) and Cluster 3 (right) observations of the 1 February 2006 patch. (a) Along-track luminosity as determined from the Resolute Bay red-line imager, where the background luminosity is deducted and a 5-min median filter is applied. The dashed lines indicate the start and end of the patch crossing (>5 R above the background). (b) E_x and E_y measurements taken from the Electron Drift Instrument (EDI), where a 90-s median filter is applied. (c) Magnetic field perturbations relative to the T01 magnetic field model, where a 30-s median filter is applied. (d) Field-aligned currents (FACs) determined from the magnetic field perturbations presented in Panel c, where a 120-s median filter is applied. Positive is upward. (e and f) Electron flux measurements parallel and antiparallel to the magnetic field, where the black curve indicates the spacecraft potential with a 90-s median filter. (g) Ion number flux parallel (black) and antiparallel (blue) to the magnetic field, where a 60-s median filter is applied.

During this patch motion, the Cluster 1 and Cluster 3 spacecraft cross the open field lines associated with the patch, from the leading/dawnward edge of the patch to the trailing/duskward edge (where leading and trailing indicate the front and back of the patch, respectively, in relation to the patch motion). Cluster 1 passes through the patch from 6:34 to 6:55 UT, while Cluster 3 passes through the patch from 6:41 to 6:56 UT. These times are determined from the along-track optical luminosity given by the imager along the satellite footprint, as shown in Figure 2a. The maximum along-track luminosity within the patch is 35 R for Cluster 1 and 25 R for Cluster 3, well above the background luminosity of ~1 R.

Figure 2b shows that dawnward of the patch edges, Cluster 1 probes a fluctuating E_y that remains within ±1 mV/m far outside the patch. Approximately 10 min prior to the dawnward edge and 20 min after the duskward edge, E_y increases up to 3 mV/m, indicating an enhanced antisunward $\mathbf{E} \times \mathbf{B}$ flow channel associated with the patch. Additionally, E_x fluctuates within ±1 mV/m prior to the dawnward edge of the patch and then changes from −1 mV/m within 10 min dawnward of the patch to above 1 mV/m approximately 5 min duskward of the patch. Approximately 10 min duskward of the patch, E_x and E_y decrease and fluctuate near zero. The behavior of E_x indicates a dawnward flow turning duskward, which is consistent with the patch optical motion and the IMF B_y turning from negative to positive.

Cluster 3 detects similar electric field signatures. After fluctuating between approximately 2 and −1 mV/m, E_y increases and peaks above 3 mV/m approximately 5 min prior to the dawnward edge of the patch. Closer to the duskward edge, E_y decreases and fluctuates around 1 mV/m. It is interesting to note that Cluster 3 shows the E_y enhancement to be more localized and stronger near the dawnward edge of the patch than

Cluster 1, indicating either a growing flow channel on the dawnward edge of the patch or a small-scale spatial structure that only Cluster 3 passes through. Prior to the dawnward edge of the patch, E_x at Cluster 3 fluctuates near −1 mV/m but then turns positive within the patch and extends above 1 mV/m within 5 min duskward of the patch. Then, E_x decreases to near zero. Similar to the Cluster 1 measurements, Cluster 3 indicates an antisunward flow channel coincident with the patch, as well as a dawnward to duskward change in the flow.

Figure 2c shows that throughout this E_y enhancement, Cluster 1 and Cluster 3 both probe overall smooth magnetic field changes with small fluctuations. Both Cluster 1 and Cluster 3 indicate a sunward B_x change within the patch compared to B_x before the patch encounter. This, combined with a duskward E_y, indicates a downward Poynting vector within the patch (see equation (3)). For Cluster 1, Figure 2d shows that the FAC is upward approximately 10 min before the dawnward edge of the patch, downward in much of the patch, and then upward toward the duskward edge of the patch (see equation (2)). Cluster 3 infers a similar FAC structure, but the FACs are smoother, and their magnitude is slightly smaller. The different levels of FAC fluctuations at the two spacecraft suggest that small-scale FACs are present or that a portion of the FACs are highly variable, while the patch-scale FAC sheets are more stable. Much of the enhanced positive E_y is located in the region of the downward and the second upward FACs. Namely, this FAC pair has a Region 1 sense, where a downward FAC is present on the dawnside of the patch and an upward FAC is present on the duskside (as done in Zou et al., 2016, the term "Region 1 sense" simply refers to the direction of the localized FAC system and does not suggest that this signature is directly connected to the large-scale Region 1/Region 2 current system). The enhanced positive E_y drives a Pedersen current to close the FACs and is characteristic of a flow channel within the FAC pair. The upward FAC dawnside of the patch may close through a portion of the downward FAC, in association with the negative E_y (Region 2 sense FAC).

Throughout the majority of the enhanced E_y, Figures 2e and 2f indicate a weakly enhanced diffuse electron energy flux both parallel and antiparallel to the magnetic field. At the dawnward edge of the patch, the electron flux increases to $\sim 3 \times 10^6$ eV cm^2·s^{-1}·sr^{-1}·eV^{-1} between approximately 20 and 500 eV, almost fully coincident with the patch. The downgoing flux is slightly larger than the upgoing flux, indicating that these electrons originate in the magnetosphere or magnetosheath. Then, a separate and larger ($\sim 1 \times 10^7$ eV cm^2·s^{-1}·sr^{-1}·eV^{-1}) electron flux enhancement is detected mostly in the second upward FAC. Note that the low-energy portion of the lower-energy flux is due to the spacecraft potential (indicated by a black line). The enhanced electron precipitation seen here is typical of polar rain, which is uniform and soft between 100 and 300 eV (Winningham & Heikkila, 1974). Meanwhile, the ion number flux averaged over ≤100 eV, shown in Figure 2g, is weakly enhanced bidirectionally near the duskward edge of the patch from about 7×10^6 cm^2·s^{-1}·sr^{-1} to over 1×10^7 cm^2·s^{-1}·sr^{-1} for both satellites. Later, more substantial upgoing ions (i.e., ion outflow) reaching nearly 7×10^7 cm^2·s^{-1}·sr^{-1} are detected in a region where the electron flux is particularly enhanced and upward FACs exist. This ion outflow may be the result of either a heating by precipitation or a pileup of ions on the duskward edge of the patch by the duskward electric field.

Figure 2 shows that Cluster 3 measures overall similar features as Cluster 1 with an approximate 5-min time lag, consistent with the patch encounter time lag. For example, E_y turns from negative to positive at 6:27 UT at Cluster 1 and 6:30 UT at Cluster 3, and the electron flux increases at 6:34 UT at Cluster 1 and 6:41 UT at Cluster 3. This time lag emphasizes that these features are not temporal changes of large-scale features but are rather localized spatial structures in the polar cap. Both spacecraft (Cluster 1 especially) show a strong correlation of a localized and enhanced E_y with a Region 1 sense FAC pair and an electron energy flux enhancement.

3.1.2. Case Study 2: 29/30 December 2005

Figure 3 and Movie S2 show a group of airglow patches moving dawnward and antisunward on 29/30 December 2005. The patches detach from the dayside auroral oval (bright region to the top) and propagate into the polar cap. During this period, the IMF B_z fluctuates between northward and southward, while the IMF B_y is predominately negative, which is consistent with the dawnward motion of the airglow patch. Although the data are somewhat noisy, plasma frequency measurements from the Resolute Bay ionosonde presented in Figure S3 show a change in the peak plasma frequency from 6.0 MHz at 23:00 UT, when the ionosonde is observing the patch of interest, to 3.5 MHz at 23:15 UT, when the ionosonde is observing the background polar cap. These observations indicate a density increase by a factor of 2.9 within the airglow structure, which means that it is a polar cap patch. Eureka ionosonde observations are not available during this period.

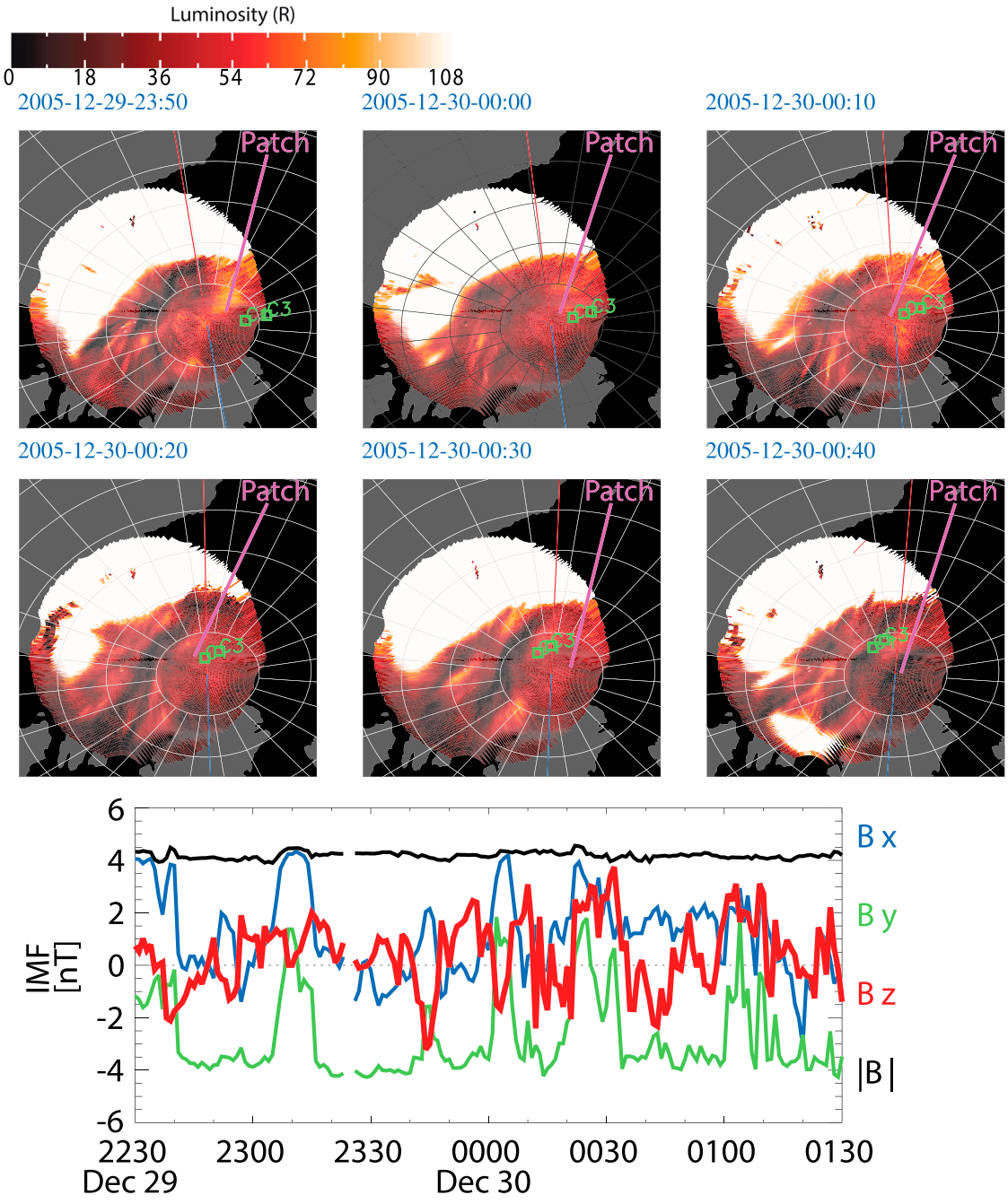

Figure 3. Red-line emission data from the Resolute Bay Optical Mesosphere Thermosphere Imagers instrument, along with the corresponding interplanetary magnetic field (IMF) conditions, for a 29/30 December 2005 airglow patch observation. Presented in the same format as Figure 1.

Figure 4 shows measurements taken from the Cluster spacecraft as they pass from the leading/dawnward edge of one of the patches to the trailing/duskward edge of the patch. Cluster 1 passes through the patch from 23:48 to 0:36 UT, while Cluster 3 passes through the patch from 23:57 to 0:41 UT. The maximum along-track luminosity within the patch is 80 R for Cluster 1 and 90 R for Cluster 3, well above the background luminosity of ~5 R.

Figure 4b shows that, prior to the patch crossing, E_y is small and fluctuates near zero. Within a 10 min period from the dawnward edge of the patch, Cluster 1 shows an enhanced E_y that extends up above 4 mV/m and then back to 2 mV/m and below. The positive E_y around the dawnward edge of the patch suggests an enhanced antisunward flow associated with the patch. Another weaker positive E_y exists at the duskward

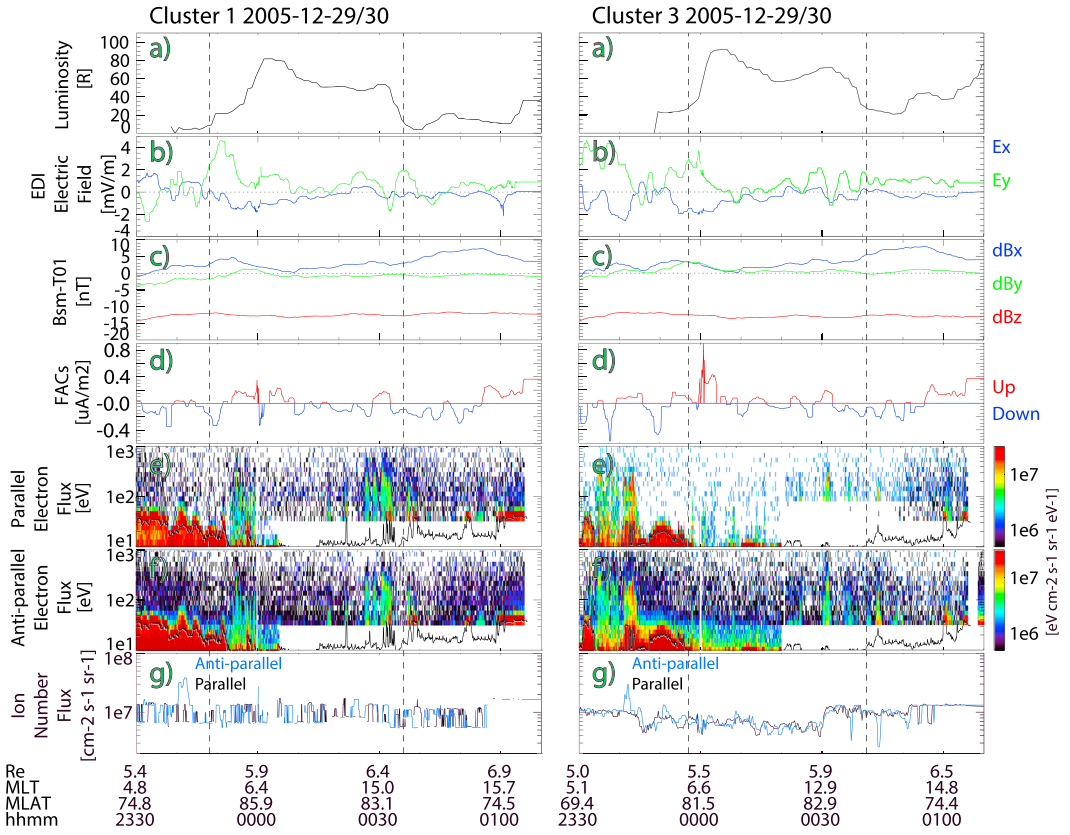

Figure 4. Cluster 1 (left) and Cluster 3 (right) observations before, during, and after the 29/30 December 2005 patch. Presented in the same format as Figure 2.

edge of the patch where E_x is also enhanced negatively. This is consistent with the dawnward motion of the patch under negative IMF B_y.

Cluster 3 shows similar E_y enhancements of ~4 mV/m at the dawnward edge of the patch and ~2 mV/m fluctuations at the duskward edge, with an ~10 min time delay from the localized E_y at Cluster 1. Consistent with Case 1, this E_y change indicates the existence of spatially localized antisunward flow channels rather than a temporal change in convection. This signature suggests that there are two antisunward flow channels associated with the patch. E_x is also negatively enhanced in this region. There is another set of enhanced electric field (and precipitation) signatures ~20 min before the Cluster 3 patch encounter. This feature is likely associated with another flow channel system outside the imager FOV.

Figure 4c shows that, throughout the patch, both Cluster 1 and Cluster 3 measure smooth magnetic field changes with small fluctuations. Once again, both Cluster 1 and Cluster 3 show a sunward dB_x at the patch edges where E_y is enhanced and duskward. This indicates a downward Poynting vector within the patch (see equation (3)). Figure 4d shows that the FAC system is found to be more variable than that observed in Case 1 (equation (2)). Cluster 1 infers a downward FAC at the dawnward edge of the patch with approximately $-0.4\ \mu A/m^2$, and then an upward FAC until the patch luminosity reaches its peak. This is a Region 1 sense FAC pair, where the enhanced E_y electric field would close Pedersen currents. After the luminosity reaches its peak, the FAC is overall downward and then becomes upward toward the end of this plotted time interval. The second pair of FACs may be related to the E_y enhancement at the duskward edge of the patch.

Figures 4e and 4f indicate that the electron energy flux increases to $\sim 4 \times 10^6$ eV $cm^2 \cdot s^{-1} \cdot sr^{-1} \cdot eV^{-1}$ between 10 and 100 eV at the dawnward edge of the patch, which is associated with the upward FACs. Another burst of precipitation is located at the duskward edge of the patch. In contrast to the diffuse electron fluxes observed in Case 1, electron fluxes in Case 2 are more localized and show a bursty nature with signatures of field-aligned acceleration, thus marking different flux tube properties. Cluster 3 observes these features as well, but the electron flux is smaller. Figure 4g indicates that the ion flux does not change at the dawnward

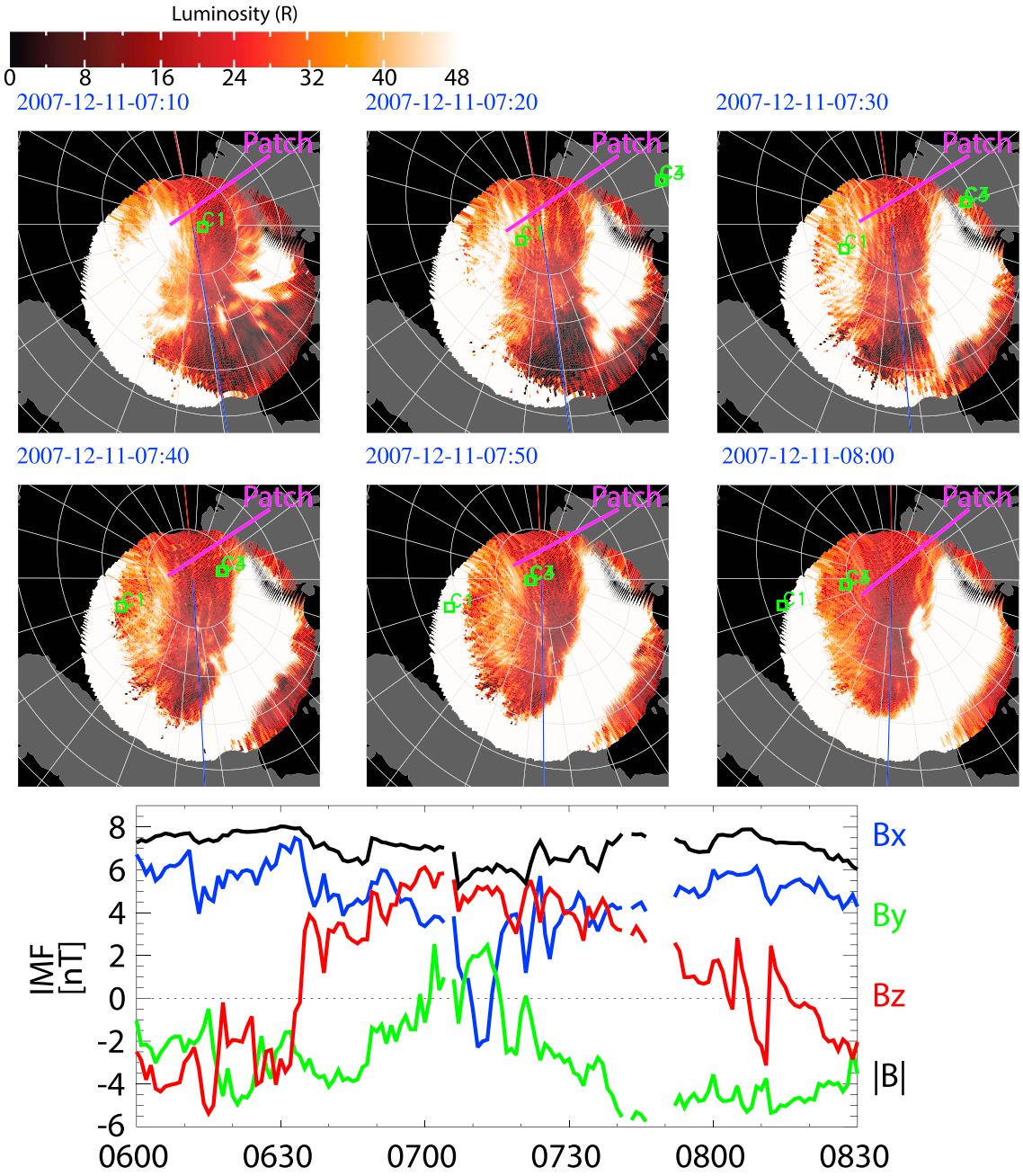

Figure 5. Red-line emission data from the Resolute Bay Optical Mesosphere Thermosphere Imagers instrument, along with the corresponding interplanetary magnetic field (IMF) conditions, for the 11 December 2007 airglow patch observation. Presented in the same format as Figure 1.

edge of the patch but shows a small increase near the duskward edge for Cluster 3. An ion outflow is seen before the encounter of the dawnward edge.

This case study supports the findings of Case 1 and also features two Region 1 sense FAC systems associated with the patch. The first system is located near the dawnward edge of the patch, while the second one is near the duskward edge. The signatures of these FAC systems are a downward and upward FAC pair coincident with an enhancement in E_y and electron flux, as observed in Case 1. However, ion outflows are not associated with the patch in this case.

3.1.3. Case Study 3: 11 December 2007

Figure 5 shows an airglow patch on 11 December 2007, along with corresponding IMF conditions. The patch initially moves dawnward and antisunward and then becomes stagnant. After brightening briefly around

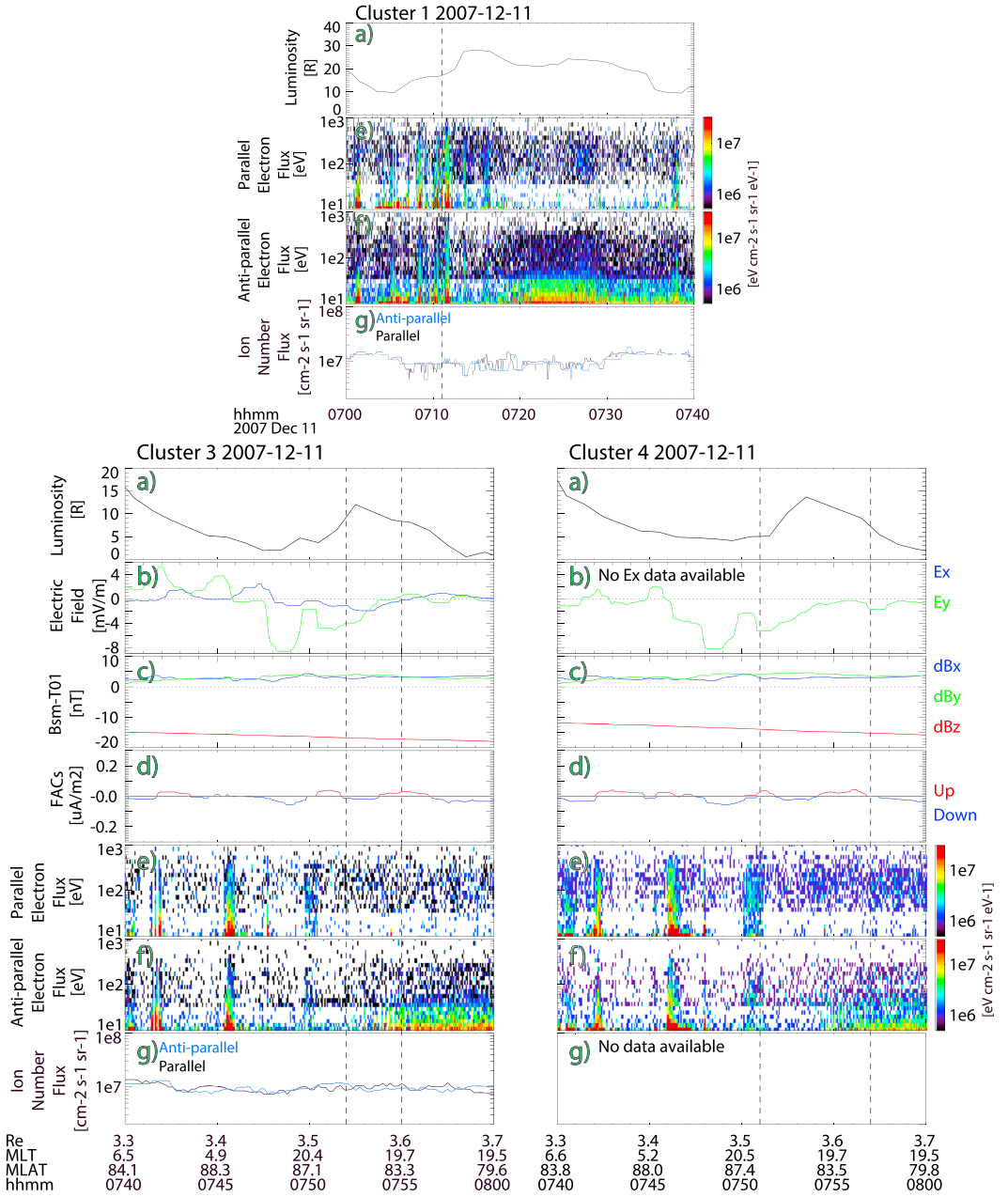

Figure 6. Cluster 1 (top), Cluster 3 (left), and Cluster 4 (right) observations before, during, and after the 11 December 2007 patch. Presented in the same format as Figure 2. Note that Cluster 1 does not have electric field, spacecraft potential, or magnetic perturbation data and Cluster 4 does not have ion data. Additionally, only the dawnward edge of the patch can be distinguished in the Cluster 1 along-track luminosity; hence, only the dawnward edge is indicated.

7:00 UT, the patch begins dissipating by the time the Cluster spacecraft pass through from the dawnside to the duskside, as seen in Movie S3. The initial motion is consistent with the southward B_z and negative B_y components of the IMF, while the stagnation is consistent with the northward turning of the IMF (Weimer, 1995). The patch of interest did not pass through either the Resolute Bay ionosonde or the Eureka ionosonde. However, similarly luminous structures observed by the Eureka and Resolute Bay ionosondes have a negligible density enhancement, indicating that these airglow patches are not necessarily polar cap patches (they satisfy the definition of an airglow patch, but not the traditional definition of a polar cap patch). Note also that during this period, a series of dawnward moving arcs are present in the imager FOV and cross the Cluster spacecraft trajectory.

The corresponding Cluster measurements are given in Figure 6, along with the along-track luminosity from the red-line imager. Since Cluster 4 EDI measurements are not available, EFW instrument measurements of E_y have been used instead. Additionally, measurements of the electric field, the spacecraft potential, and the magnetic field are not available from Cluster 1 in this case; thus, only electron and ion flux measurements are provided by Cluster 1.

Cluster 1 enters the patch at 7:11 UT, and although it is unclear exactly when Cluster 1 exits the patch (since it begins to merge with the bright auroral oval), the maximum luminosity around this time is 30 R, and the background luminosity is ~10 R. After passing through a polar cap arc, Cluster 3 passes through the patch from 7:52 to 7:55 UT, and Cluster 4 passes through the patch from 7:51 to 7:57 UT. The maximum along-track luminosity within the patch is ~10 R for both Cluster 3 and Cluster 4, and the background luminosity is ~3 R. Note that the maximum along-track luminosity decreases from Cluster 1 to Cluster 3 and Cluster 4, demonstrating that, over time, this patch is subject to a decay due to recombination. Also note that the along-track luminosity of this patch (particularly along the Cluster 3 and Cluster 4 tracks) is less than those in either Cases 1 or 2. This indicates that when the Cluster spacecraft traveled through this patch, there was less density present in the ionosphere than when the spacecraft traveled through the patches in Cases 1 and 2.

Figure 6b indicates that prior to the dawnward edge of the patch; both Cluster 3 and Cluster 4 observe an approximately −8 mV/m E_y that is coincident with the polar cap arc. Inside and on the duskside of the patch, E_y is negative and close to zero, without any substantial positive E_y. This contrasts Cases 1 and 2, where a distinct positive E_y is present over the patches. Figure 6c shows that the the change in magnetic perturbation is relatively minimal; therefore, the Poynting vector is very small. FAC fluctuations shown in Figure 6d are within ±0.1 μA/m^2, considerably less than the FACs found in Cases 1 and 2 (approximately −0.2 to 0.1 μA/m^2 for Case 1 and −0.4 to 0.8 μA/m^2 for Case 2). Thus, neither a Region 1 sense or a Region 2 sense FAC pair can be attributed to this patch.

The Cluster spacecraft all show electron energy flux enhancements of the patch in association with the auroral oval and the observed polar cap arc. Duskward of the dawnward edge of the patch, Cluster 1 does not show much of an enhancement of electron fluxes parallel to the magnetic field, and only a <100 eV enhancement of electron flux antiparallel to the magnetic field. Meanwhile, when the Cluster 3 and Cluster 4 satellites cross through the patch, there is relatively little enhancement from the background energy flux inside the airglow patch. Duskward of the patch, Cluster 3 and Cluster 4 record the same electron flux signature viewed in Cluster 1 data, indicating that the <100 eV enhancement antiparallel to the magnetic field is associated with the auroral oval. Therefore, throughout this period, there is no significant electron flux enhancement that can be attributed to the patch.

Contrary to Cases 1 and 2, this case shows a patch with no enhanced features in electric field, FACs, electron flux, or ion flux. As discussed in the next section, the difference in magnetospheric structures in Case 3 indicates the much slower motion of the patch.

3.1.4. Case Study Summary

Three case studies have been presented: two in which the patches are moving during the satellite crossings and one in which the patch stagnates and begins dissipating before the satellite crossings. Arguably, the most striking feature associated with the patches presented in Cases 1 and 2 is the localized E_x and E_y on the patch field lines. E_y in particular is enhanced at the leading edge (dawnward edge) of the patches. These signatures are coincident with localized Region 1 sense FAC pairs, namely, a downward FAC on the dawnside and upward FAC on the duskside. This is consistent with a positive E_y closing the localized FAC pairs through Pedersen currents. Although these two cases detected enhancements in electron flux related to the patch, the electron flux is diffuse for Case 1 and bursty for Case 2, indicating different flux tube properties between Cases 1 and 2. Note that we do not suggest that these patches were created from an enhanced electron flux. Case 1 shows a weak precipitation coinciding with the luminosity enhancement, but the stronger precipitation from 7:10 to 7:30 UT overlaps with only a <5 R luminosity. Meanwhile, the luminosity enhancement in Case 2 is much wider than the localized precipitation. Both Cases 1 and 2 also show a comparable level of both upgoing and downgoing electron fluxes, indicating that the majority of the downgoing fluxes is being reflected without reaching the ionosphere. The ion number flux also changes in relation to the patch, but this is less predictable than the electron energy flux.

Case 3, on the other hand, shows that when the patch begins to slow down and ultimately disappear, there are no significant lobe structures associated with the patch. Since the patch luminosity is an indication of patch age, one can conclude that the patch visited in Case 3 is older than in either Cases 1 or 2. Therefore, older patches do not possess the clear lobe structures that younger patches have. The lack of E_y lobe structures in Case 3 also indicates that the patch is moving more slowly than the patches in Cases 1 and 2, which is not just consistent with imager data but also indicates a lack of enhanced ionospheric flow channels. These findings are consistent with Ma et al. (2018), who show that patches closer to their initial creation phase are more likely to be associated with particle precipitation and plasma flows.

3.2. Superposed Epoch Analysis

Using the definition of a patch presented in section 2.1, 38 patch crossings by Cluster satellites were identified between 2005 and 2009. From these events, a superposed epoch analysis is performed to examine if lobe electric field, FAC, and particle flux features are commonly associated with patches. Since the Cluster spacecraft encounter the field lines associated with airglow patches at different altitudes from pass to pass, passes that occur at higher altitudes in the magnetosphere detect weaker electric field and FAC structures than those that occur closer to the ionosphere. To correct this altitude effect, the electric field is scaled to its magnitude at 250 km altitude using Mozer (1970)

$$\frac{E_{Ni}}{E_{Ne}} = 2L(L - 3/4)^{1/2} \tag{4}$$

and

$$\frac{E_{Wi}}{E_{We}} = L^{3/2}, \tag{5}$$

where E_W is the electric field component in the east-west direction; E_N is the electric field component in the north-south direction; the subscripts i and e refer to quantities measured in the ionosphere and at the equator, respectively; and L denotes L-shell. Knowing the distance between dipole field lines in both the meridional and zonal directions at both ionospheric and magnetospheric distances, the FACs are scaled according to the change in the flux tube cross-section area. The particle flux data cannot reasonably be scaled in a similar fashion because some particles have mirror points above the ionosphere and may also experience nonadiabatic wave-particle interactions. Therefore, the particle flux data are not mapped to the ionosphere.

In Figure 7, the time at which each satellite encounters the dawnward edge of each patch is defined to be the epoch time zero, such that anything before this time is dawnward of the patch and anything after is either within or duskward of the patch. Figure 7 shows the resulting 25th percentile (red line), median (black line), and 75th percentile (blue line) of the epoch study. Periods in which the Cluster satellites traveled through arcs or the auroral oval, as well as periods in which a given Cluster satellite is outside the imager FOV, are removed from individual passes. In addition, the median and quartiles are only calculated if they are based on more than two passes.

This dawnward edge epoch study contains the 33 satellite passes in which the dawnside edge is clearly identifiable (i.e., no other adjacent optical structures or light contamination is observed). Of these passes, 27 contain moving patches and 6 contain stagnant patches. Of the 27 passes containing moving patches, 17 patches are moving dawnward, and 10 are moving duskward, while 20 patches are moving antisunward, and 4 patches are moving sunward (3 are moving purely duskward). As expected, the dawnward moving patches typically occur under $-B_y$ conditions, while the duskward moving patches typically occur under $+B_y$ conditions.

The along-track luminosity in Figure 7a shows the patch size is variable, but the median suggests that a typical patch-crossing time along the satellite track is ~30 min, where the median luminosity reaches ~16 R above the background luminosity. Based on the approximate altitude and the patch duration, the patch width is 1.2 Earth radii in the lobe and 700 km in the ionosphere, which is consistent with Crowley (1996).

The median FAC in Figure 7b is downward at the dawnward edge, and upward from 20 to 30 min in epoch time, which is near the duskward edge of the patch. The quartiles follow a similar trend. This downward FAC on the dawnward side and upward FAC on the duskward side is consistent with the Region 1 sense FAC signatures seen in Cases 1 and 2. These findings are consistent with those from Zou et al. (2016), who also found FACs collocated with patches to typically feature a Region 1 sense.

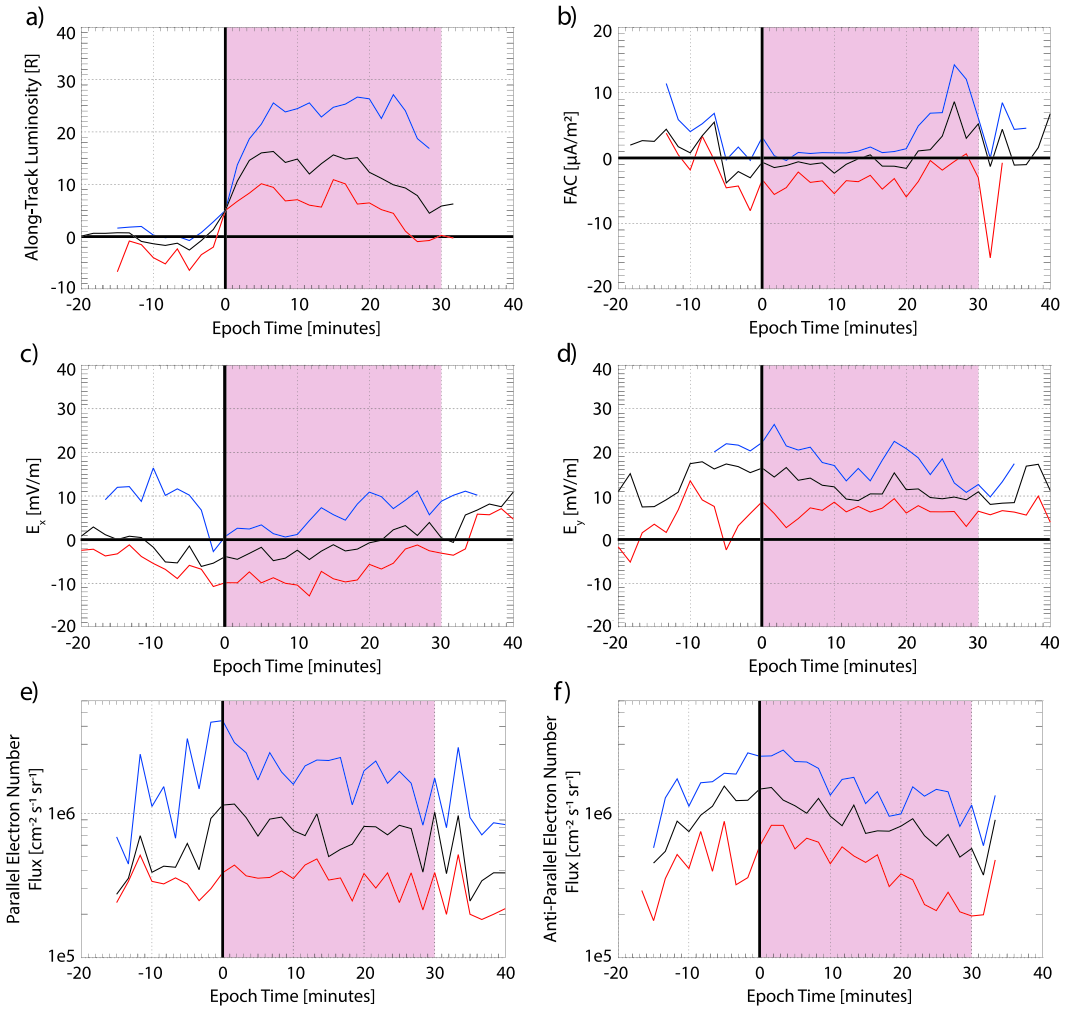

Figure 7. Superposed epoch studies performed with respect to the dawnward edge of each patch, where the red line is the 25 percentile, the black line is the median, and the blue line is the 75 percentile. The shaded purple region indicates the approximate patch width. (a) Along-track luminosity, where the dawnward edge is normalized to 5 R. (b) Field-aligned current at 250 km. (c) E_x at 250 km. (d) E_y at 250 km. (e) Parallel electron number flux at the Cluster spacecraft altitudes. (f) Antiparallel electron number flux at the Cluster spacecraft altitudes.

Figure 7c shows that, around the dawnward edge, the median E_x ranges between −10 and 0 mV/m from −10 to 20 min, indicating an overall dawnward motion. This is consistent with the dawnward motion of the majority of the patches. Meanwhile, Figure 7d shows that E_y is positive throughout the patch. E_y increases at approximately −10 min in epoch time and peaks near 0 min. A smaller peak exists at 20 min, around the duskward edge of the patch. This study is consistent with Case 2 and could indicate the presence of multiple mesoscale flow channels within a given patch.

Figures 7e and 7f show that both the electron flux parallel and antiparallel to the magnetic field are elevated at the dawnward edge of the patch relative to background energy flux, which is consistent with what is seen in Cases 1 and 2. From the initial jump at the dawnward edge to the duskward side, the electron flux decreases gently, indicating a strong degree of collocation between the electron flux and the patch that varies in position from pass to pass. Since the antiparallel flux is comparable to the parallel flux, much of the electron flux sent toward the ionosphere reflects back rather than being lost.

An additional superposed epoch study is given in Figure 8 using the leading edge of the patch as the zero epoch time, such that everything before epoch time zero is in front of the leading edge of the patch and everything after is either within or trailing the patch. Note that because the leading edge cannot be defined for stagnant patches (e.g., Case 3), this study is based on 27 passes where the patch motion and leading edge

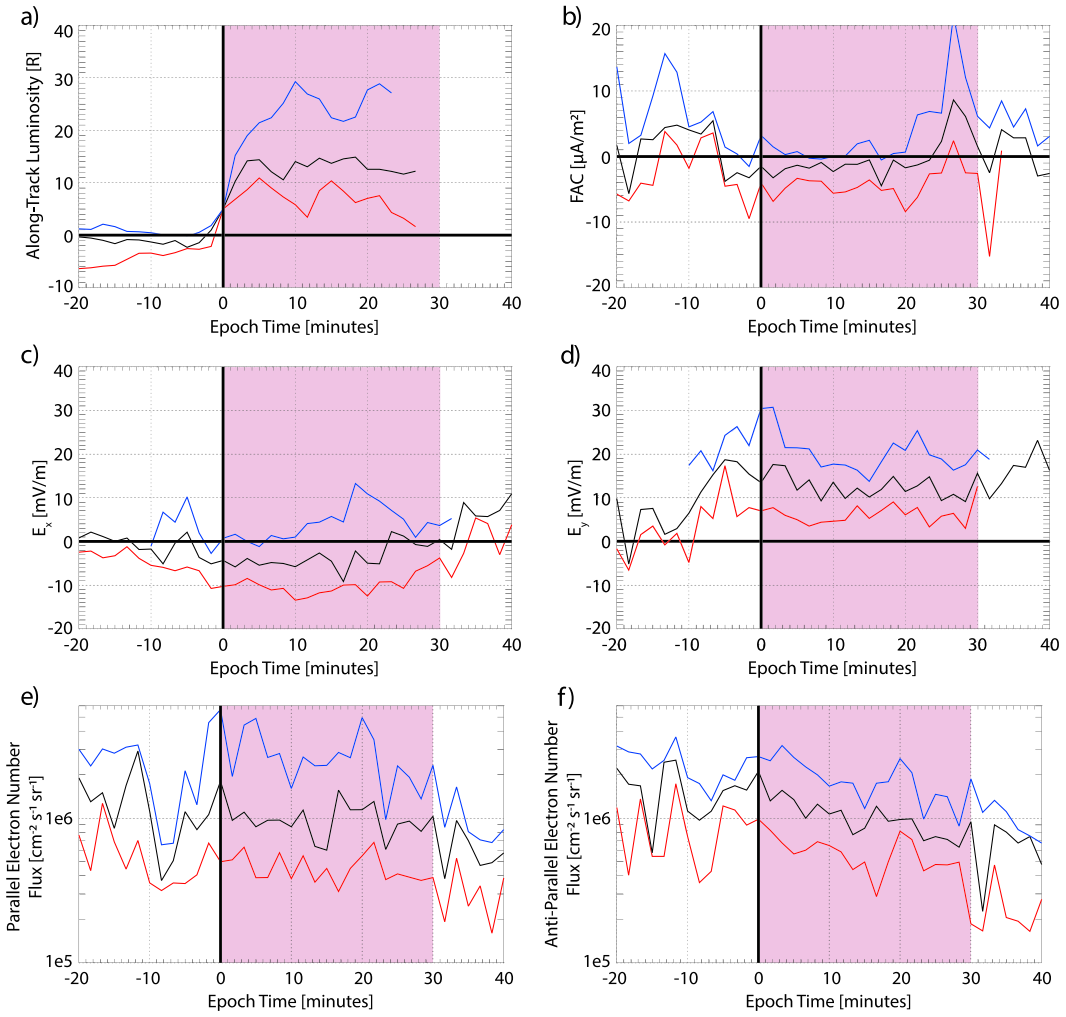

Figure 8. Superposed epoch studies performed with respect to the leading edge of each patch, where the red line is the 25 percentile, the black line is the median, and the blue line is the 75 percentile. The shaded purple region indicates the approximate patch width. (a) Along-track luminosity, where the leading edge is normalized to 5 R. (b) Field-aligned current at 250 km. (c) E_x at 250 km. (d) E_y at 250 km. (e) Parallel electron number flux at the Cluster spacecraft altitudes. (f) Antiparallel electron number flux at the Cluster spacecraft altitudes.

are clearly visible in the imager data. In this study, 19 of the passes show dawnward moving patches, while 8 show duskward moving patches. Twenty-two passes contain antisunward moving patches, while two are sunward. Lastly, 14 of the 27 leading edges are also the dawnward edge, while the remainder are duskward, leading edges.

The along-track luminosity in Figure 8a shows a luminosity peak similar to that in the dawnward edge epoch study (Figure 7a). Data after 30 min are still mostly in the polar cap but are not shown because the data become somewhat noisy and the number of samples is limited. Therefore, the trailing edge is not clear in this plot, and the patch width is simply taken to be the same as that seen in the dawnward edge epoch study. In the FAC epoch study given in Figure 8b, the median FAC at the leading edge is negative and then upward after ~25 min epoch time. This population is consistent with the FAC structure seen in Cases 1 and 2, where the leading/dawnward edge shows a downward FAC and the trailing/duskward edge shows an upward FAC.

Throughout the patches, the epoch E_x in Figure 8c is negative and fluctuates between −10 and 20 min epoch time, similar to the dawnward side epoch E_x (Figure 7c). This trend properly indicates that slightly more than half of the patches drift dawnward, while the rest of the patches drift duskward. Meanwhile, Figure 8d shows a distinct 20 mV/m enhancement of E_y near the leading edge compared to the background electric field. E_y decreases closer to the trailing edge but maintains a larger percentile spread than the duskward edge in the

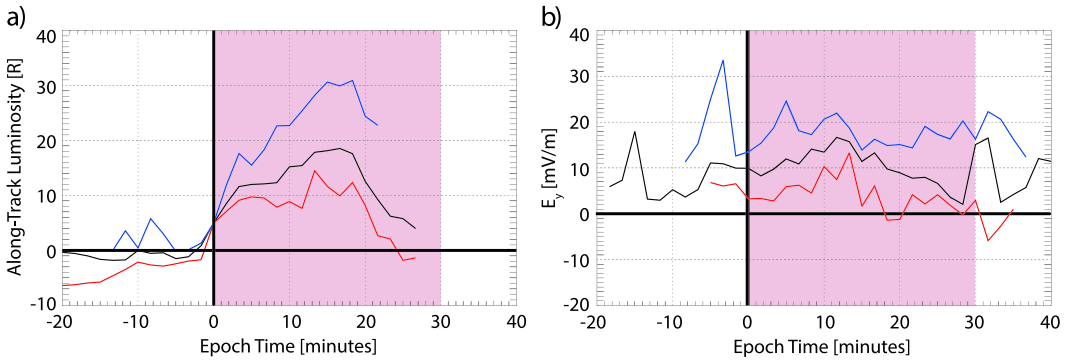

Figure 9. Superposed epoch studies performed with respect to the duskward edge of each patch, where the red line is the 25 percentile, the black line is the median, and the blue line is the 75 percentile. The shaded purple region indicates the approximate patch width. (a) Along-track luminosity, where the dawnward edge is normalized to 5 R. (b) E_y at 250 km.

dawnward edge epoch study. This suggests that E_y enhancements are more localized with the leading edge than the trailing edge, while the dawnward edge superposed epoch study suggests that E_y enhancements are localized with either the duskward edge or the dawnward edge.

The electron number flux in Figures 8e and 8f for the leading edge epoch study is similar to those from the dawnside epoch study (Figures 7e and 7f). More specifically, the leading edge shows an increase in the electron number flux both parallel and antiparallel to the magnetic field that decreases gently throughout the patch. This indicates that the collocation of the electron number flux with the patch is not more strongly dependent on the leading edge than the dawnward edge, or vice versa.

Figure 9 presents a final brief epoch study in which epoch time zero is taken to be the duskward edge, implying any time after zero is dawnward. This study contains 31 satellite passes in which the duskside edge is clearly identifiable. Of the 25 passes containing moving patches, 16 patches are moving dawnward, and 9 patches are moving duskward, while 18 patches are moving antisunward, and 4 patches are moving sunward (three patches are moving purely duskward). These results are noisier than the previous studies; therefore, only the along-track luminosity and E_y are presented. The along-track luminosity in Figure 9a suggests that the patch crossing time could be between 20 and 30 min. Meanwhile, E_y shows multiple peaks, indicating that both the dawnward and duskward epoch studies show the presence of multiple E_y structures. Overall, the results of the duskward edge epoch study are consistent with both the dawnward edge and leading edge epoch studies.

The epoch studies presented in this paper show the typical structures to which airglow patches in the ionosphere map to in the magnetosphere. These are consistent with Cases 1 and 2. These results demonstrate that localized enhancements in E_x and E_y, indicating the presence of flow channels, and localized Region 1 sense FACS are commonly associated with moving airglow patches. An enhanced electron flux is also tied to the lobe structures.

3.3. Airglow Patches and FAC Drivers

The polar cap studies mentioned in section 1 infer that past observations of enhanced electric field, electron flux, and FAC structures collocated with airglow patches are driven by the magnetosphere. The present study provides evidence that such structures exist in the magnetosphere and indicates the presence of a magnetospheric driver. This driver is most likely magnetopause reconnection, which opens magnetic field lines and transports plasma faster than the surrounding flux tubes. The resulting enhanced lobe electric fields and Region 1 sense FAC structures are consistent with the fast flow channels typically associated with patches in the ionosphere and imply the presence of a Pedersen current within the patch. In turn, these enhanced FACs are also consistent with the enhanced particle fluxes associated with patches, both within the ionosphere and their lobe structures, which make the characteristics of airglow patch flux tubes distinct from the surrounding flux tubes. This implies that the enhanced precipitation of airglow patches is a remnant population of cusp/cleft precipitation.

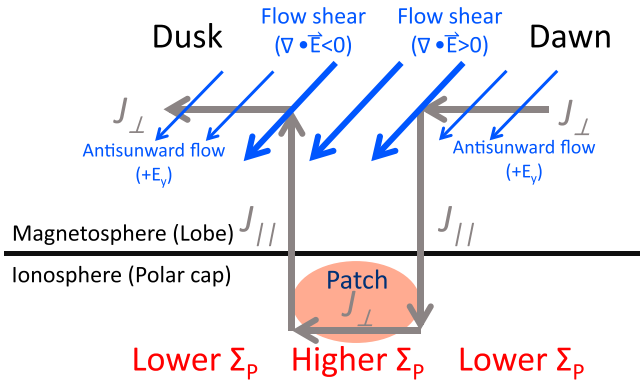

Figure 10. Diagram of one possible current and flow system associated with airglow patches, particularly younger patches.

Based on the presented Cluster observations, Figure 10 illustrates one possible dynamo region flow and current system associated with patches. The flow shear at the edge of the patch results in either the convergence or divergence of the electric field mainly in the dusk-dawn direction, where a converging electric field drives an upward FAC, and a diverging electric field drives a downward FAC. Note that this is similar to Sun-aligned arcs, as discussed in Shiokawa et al. (1996) and references therein. The present study shows that a similar flow and current system can exist on open field lines without large precipitation under the southward IMF.

While we consider that the measured electric field structures are driven by the magnetosphere, it is worthwhile examining if those could also be driven within the ionosphere by either a neutral wind dynamo, or a GDI dynamo. From Schunk and Nagy (2009), the Pedersen current within the ionosphere is written as

$$\mathbf{J}_P = \Sigma_P \left(\mathbf{E}_i + \mathbf{U} \times \mathbf{B} \right), \tag{6}$$

where $\mathbf{U}$ is the neutral wind, $\mathbf{E}_i$ is the electric field in the ionosphere, and Σ_P is the Pedersen conductance. Assuming a typical background antisunward wind of $U \approx 150$ m/s due to the thermospheric pressure bulge imparted by dayside solar heating (e.g., Killeen et al., 1982), $\mathbf{U} \times \mathbf{B}$ is less than 20 mV/m dawnward. This indicates that, due to the neutral wind, the Pedersen current is dawnward. Cross-track Challenging Minisatellite Payload (CHAMP) observations of Case 1 (nearly dawn-dusk orbit not shown) suggest a 50 m/s duskward U (sunward-antisunward measurements are not available), and thus an ~3 mV/m antisunward $\mathbf{U}\times\mathbf{B}$. However, this contribution is significantly less than the dawnward $\mathbf{U}\times\mathbf{B}$ contribution to the Pedersen current.

However, within a plasma density enhancement, Σ_P is elevated. This means that, within the patch, the Pedersen current results in an accumulation of electrons on the duskward side of the patch and an accumulation of ions on the dawnward side. This leads to (1) an upward FAC on the dawnside of the patch, (2) a downward FAC on the duskside of the patch, and (3) a duskward polarization electric field. Although this duskward polarization electric field is consistent with the Cluster observations reported here, the FAC system established by the neutral wind dynamo is of a Region 2 sense instead of the observed Region 1 sense. This reversed FAC current system then results in an antisunward B_x within the patch through Ampere's law, meaning that equation (3) results in an upward Poynting flux from a $-B_x$ component and a $+E_y$ polarization electric field. This reversed Poynting flux also contradicts the observations presented in this paper.

As mentioned previously, the GDI is also believed to create the current and electric field structures associated with polar cap patches. Through the GDI, multiple fluctuating regions of ion and electron buildups result along the trailing edge of a given patch, as well as varying dawnward and duskward electric fields and Region 1 sense and Region 2 sense FAC pairs. Although this mechanism therefore results in both duskward electric fields and Region 1 sense FACs, the dawnward electric fields are coincident with Region 1 sense FACs, and duskward electric fields are coincident with Region 2 sense FACs, which is inconsistent with Cluster observations. Additionally, these FAC current systems result in magnetic field perturbations that are sunward during Region 1 sense FACs and antisunward during Region 2 sense FACs. This variation in magnetic field contradicts the observations made by the Cluster satellites. In addition, considered concurrently with the electric field variations, the magnetic field variation results in a consistently upward Poynting vector, which also contradicts our results. Therefore, the magnetospheric signatures of patches are driven by the magnetosphere through such mechanisms discussed in Nishimura and Lyons (2016) and are not the result of either a neutral wind dynamo or a GDI dynamo.

4. Conclusions

This study uses Cluster spacecraft observations to characterize lobe structures associated with airglow patches on open field lines. Using the Resolute Bay imager to identify airglow patches, three case studies are presented. Cases 1 and 2 show enhanced duskward E_y signatures, Region 1 sense FAC pairs, a downward Poynting flux, and field-aligned electron flux signatures that are coincident with airglow patches. These enhancements are localized and correspond most strongly to the leading/dawnward edge. Two successive

satellite passes measure similar structures with a time lag, indicating that these are spatially localized structures. These features are consistent with a FAC pair being created in the magnetosphere and closing in the ionosphere through a Pedersen current. Additionally, changes in E_x correspond to changes in the dawn-dusk motion, as well as changing IMF conditions. Meanwhile, Case 3 features a patch that drifts much slower and is dissipating in luminosity and disappearing, which means that the patch is relatively old. Since Case 3 shows no significant enhancements in E_x, E_y, FACs, electron flux, or ion flux, these results indicate that the magnetospheric structures on the patch field lines are physically connected to the patch motion and that MI coupling structures observed in the lobe are the strongest when the patch propagates faster or when the patch is younger, as is consistent with Ma et al. (2018).

In total, 38 patch crossings by Cluster satellites were identified between 2005 and 2009. These measurements are used to compile a dawnside epoch study, a leading edge epoch study, and a duskward epoch study. The epoch studies performed are consistent with Cases 1 and 2 and show a strong correlation between airglow patches and enhancements in E_x, E_y, and electron flux. Additionally, Region 1 sense FACs are consistently found, indicating that observations of enhanced flows, FACs, and precipitation made by Zou et al. (2016, 2017) at ionospheric altitudes extend up into the magnetosphere. The patch width resolved from these epoch studies is also similar to that of previous patch studies.

Soft electron precipitation over the patches also supports the idea that the patch field lines have different properties than the surrounding field lines. While it is unclear what the exact cause of the two different types of observed precipitations are (diffuse vs. structured), structured precipitation suggests electron acceleration along magnetic field lines by an electrostatic potential drop or by waves, similar to polar cap arcs. However, the flux observed in this study is smaller than that for polar cap arcs, and the imagers do not show any evidence of emission directly driven by this precipitation.

The results presented in this paper are consistent with magnetopause reconnection, which opens magnetic field lines and transports plasma across the polar cap faster than the surrounding flux tubes and background plasma. Given that the Cluster observations indicate that patches are associated with Region 1 sense FAC structures and a downward Poynting flux, this work contradicts the notion that the source of the lobe features associated with patches are generated in the ionosphere. The results of this study are therefore important for our understanding of mesoscale magnetospheric forcing on open magnetic field lines and ion-neutral coupling within patches (such as that discussed in Zou et al., 2018).

Acknowledgments
This work was supported by NASA Grants NNX17AL22G and 80NSSC18K0657 and NSF Grants PLR-1341359, AGS-1737823, and AFOSR FA9559-16-1-0364. The Resolute Bay imager data are supported by the NSF Grant ATM-0608577 and a Grant-in-Aid for Scientific Research (16403007, 19403010, 20740282, 15H05815, and 16H06286) of Japan Society for the Promotion of Science (JSPS), Japan. We thank K. Hosokawa for useful discussions and his support on the Resolute Bay imager. We thank support from the CEDAR workshop "Grand Challenge: Multi scale I-T system dynamics" and ISSI workshop "Multiple-instrument observations and simulations of the dynamical processes associated with polar cap patches/aurora and their associated scintillations." Data from the Resolute Bay imager, the Cluster spacecraft, solar wind information, and the Eureka and Resolute Bay ionosondes can be retrieved online (from http://vt.superdarn.org/tiki-index.php?page=DaViT+ASI, http://cluster.irap.omp.eu/main, https://omniweb.gsfc.nasa.gov/, and http://chain.physics.unb.ca/chain/, respectively).

References

Balogh, A., Carr, C. M., Acuna, M., Dunlop, M., Beek, T., Brown, P., et al. (2001). The Cluster Magnetic Field Investigation: Overview of in-flight performance and initial results. *Annales Geophysicae*, *19*(10/12), 1207–1217. https://doi.org/10.5194/angeo-19-1207-2001

Basu, S., Basu, S., Chaturvedi, P., & Bryant, C. (1994). Irregularity structures in the cusp/cleft and polar cap regions. *Radio science*, *29*(1), 195–207. https://doi.org/10.1029/93RS01515

Basu, S., Basu, S., MacKenzie, E., Coley, W., Sharber, J., & Hoegy, W. (1990). Plasma structuring by the gradient drift instability at high latitudes and comparison with velocity shear driven processes. *Journal of Geophysical Research*, *95*(A6), 7799–7818. https://doi.org/10.1029/JA095iA06p07799

Buchau, J., Weber, E., Anderson, D., Carlson, H. Jr., Moore, J., Reinisch, B., & Livingston, R. (1985). Ionospheric structures in the polar cap: Their origin and relation to 250-mHz scintillation. *Radio Science*, *20*(3), 325–338. https://doi.org/10.1029/RS020i003p00325

Carlson, H., Moen, J., Oksavik, K., Nielsen, C., McCrea, I., Pedersen, T., & Gallop, P. (2006). Direct observations of injection events of subauroral plasma into the polar cap. *Geophysical Research Letters*, *33*, L05103. https://doi.org/10.1029/2005GL025230

Carlson, H. C., Oksavik, K., Moen, J., & Pedersen, T. (2004). Ionospheric patch formation: Direct measurements of the origin of a polar cap patch. *Geophysical Research Letters*, *31*, L08806. https://doi.org/10.1029/2003GL018166

Crowley, G. (1996). Critical review of ionospheric patches and blobs. *Review of Radio Science, 1993–1996* (619–648.

Dungey, J. W. (1961). Interplanetary magnetic field and the auroral zones. *Physical Review Letters*, *6*(2), 47–48. https://doi.org/10.1103/PhysRevLett.6.47

Foster, J. C. (1984). Ionospheric signatures of magnetospheric convection. *Journal of Geophysical Research*, *89*(A2), 855–865. https://doi.org/10.1029/JA089iA02p00855

Foster, J., Coster, A., Erickson, P., Holt, J., Lind, F., Rideout, W., et al. (2005). Multiradar observations of the polar tongue of ionization. *Journal of Geophysical Research*, *110*, A09S31. https://doi.org/10.1029/2004JA010928

Fukunishi, H., Fujii, R., Kokubun, S., Tohyama, F., Mukai, T., & Oya, H. (1991). Small-scale field-aligned currents observed by the Akebono (EXOS-D) satellite. *Geophysical Research Letters*, *18*(2), 297–300. https://doi.org/10.1029/91GL00036

Goodwin, L., Iserhienrhien, B., Miles, D. M., Patra, S., van der Meeren, C., Buchert, S. C., et al. (2015). Swarm in situ observations of F region polar cap patches created by cusp precipitation. *Geophysical Research Letters*, *42*, 996–1003. https://doi.org/10.1002/2014GL062610

Gustafsson, G., André, M., Carozzi, T., Eriksson, A. I., Fälthammar, C.-G., Grard, R., et al. (2001). First results of electric field and density observations by Cluster EFW based on initial months of operation. *Annales Geophysicae*, *19*(10/12), 1219–1240. https://doi.org/10.5194/angeo-19-1219-2001

Heelis, R. (1984). The effects of interplanetary magnetic field orientation on dayside high-latitude ionospheric convection. *Journal of Geophysical Research*, *89*(A5), 2873–2880. https://doi.org/10.1029/JA089iA05p02873

Heelis, R., Lowell, J. K., & Spiro, R. W. (1982). A model of the high-latitude ionospheric convection pattern. *Journal of Geophysical Research*, *87*(A8), 6339–6345. https://doi.org/10.1029/JA087iA08p06339

Hosokawa, K., Kashimoto, T., Suzuki, S., Shiokawa, K., Otsuka, Y., & Ogawa, T. (2009). Motion of polar cap patches: A statistical study with all-sky airglow imager at Resolute Bay, Canada. *Journal of Geophysical Research*, *114*, A04318. https://doi.org/10.1029/2008JA014020

Hosokawa, K., Shiokawa, K., Otsuka, Y., Nakajima, A., Ogawa, T., & Kelly, J. (2006). Estimating drift velocity of polar cap patches with all-sky airglow imager at resolute bay, canada. *Geophysical Research Letters*, *33*, L15111. https://doi.org/10.1029/2006GL026916

Jayachandran, P. T., Langley, R. B., MacDougall, J. W., Mushini, S. C., Pokhotelov, D., Hamza, A. M., et al. (2009). Canadian High Arctic Ionospheric Network (CHAIN). *Radio Science*, *44*, RS0A03. https://doi.org/10.1029/2008RS004046

Kelley, M. C., Vickrey, J. F., Carlson, C., & Torbert, R. (1982). On the origin and spatial extent of high-latitude F region irregularities. *Journal of Geophysical Research*, *87*(A6), 4469–4475. https://doi.org/10.1029/JA087iA06p04469

Killeen, T. L., Hays, P., Spencer, N. W., & Wharton, L. (1982). Neutral winds in the polar thermosphere as measured from Dynamics Explorer. *Geophysical Research Letters*, *9*(9), 957–960. https://doi.org/10.1029/GL009i009p00957

Kivanç, Ö., & Heelis, R. A. (1997). Structures in ionospheric number density and velocity associated with polar cap ionization patches. *Journal of Geophysical Research*, *102*(A1), 307–318. https://doi.org/10.1029/96JA03141

Lockwood, M., & Carlson, H. (1992). Production of polar cap electron density patches by transient magnetopause reconnection. *Geophysical Research Letters*, *19*(17), 1731–1734. https://doi.org/10.1029/92GL01993

Lockwood, M., Fazakerley, A., Opgenoorth, H., Moen, J., Van Eyken, A., Dunlop, M., et al. (2001). Coordinated Cluster and ground-based instrument observation of transient changes in the magnetopause boundary layer during an interval of predominantly northward IMF: Relation to reconnection pulses and FTE signatures. *Annales Geophysicae*, *19*(10), 1613–1640. https://doi.org/10.5194/angeo-19-1613-2001

Lockwood, M., Moen, J., Van Eyken, A., Davies, J., Oksavik, K., & McCrea, I. (2005). Motion of the dayside polar cap boundary during substorm cycles: I. Observations of pulses in the magnetopause reconnection rate. *Annales Geophysicae*, *23*(11), 3495–3511. https://doi.org/10.5194/angeo-23-3495-2005

Lockwood, M., Opgenoorth, H., Van Eyken, A., Fazakerley, A., Bosqued, J., Denig, W., et al. (2001). Coordinated Cluster, ground-based instrumentation and low-altitude satellite observations of transient poleward-moving events in the ionosphere and in the tail lobe. *Annales Geophysicae*, *19*(10), 1589–1612. https://doi.org/10.5194/angeo-19-1589-2001

Lyons, L., Nishimura, Y., Kim, H.-J., Donovan, E., Angelopoulos, V., Sofko, G., et al. (2011). Possible connection of polar cap flows to pre-and post-substorm onset PBIs and streamers. *Journal of Geophysical Research*, *116*, A12225. https://doi.org/10.1029/2011JA016850

Ma, Y.-Z., Zhang, Q.-H., Xing, Z.-Y., Heelis, R. A., Oksavik, K., & Wang, Y. (2018). The ion/electron temperature characteristics of polar cap classical and hot patches and their influence on ion upflow. *Geophysical Research Letters*, *45*, 8072–8080. https://doi.org/10.1029/2018GL079099

MacDougall, J. W., & Jayachandran, P. T. (2007). Polar patches: Auroral zone precipitation effects. *Journal of Geophysical Research*, *112*, A05312. https://doi.org/10.1029/2006JA011930

McWilliams, K., Yeoman, T., & Provan, G. (2000). A statistical survey of dayside pulsed ionospheric flows as seen by the CUTLASS Finland HF radar. *Annales Geophysicae*, *18*(4), 445–453. https://doi.org/10.1007/s00585-000-0445-8

Moen, J., Carlson, H., Oksavik, K., Nielsen, C., Pryse, S., Middleton, H., et al. (2006). EISCAT observations of plasma patches at sub-auroral cusp latitudes. *Annales Geophysicae*, *24*(9), 2363–2374. https://doi.org/10.5194/angeo-24-2363-2006

Moen, J., Oksavik, K., Abe, T., Lester, M., Saito, Y., Bekkeng, T., & Jacobsen, K. (2012). First in-situ measurements of HF radar echoing targets. *Geophysical Research Letters*, *39*, L07104. https://doi.org/10.1029/2012GL051407

Mozer, F. (1970). Electric field mapping in the ionosphere at the equatorial plane. *Planetary and Space Science*, *18*(2), 259–263. https://doi.org/10.1016/0032-0633(70)90161-3

Nishimura, Y., & Lyons, L. (2016). Localized reconnection in the magnetotail driven by lobe flow channels: Global MHD simulation. *Journal of Geophysical Research: Space Physics*, *121*, 1327–1338. https://doi.org/10.1002/2015JA022128

Nishimura, Y., Lyons, L., Shiokawa, K., Angelopoulos, V., Donovan, E., & Mende, S. (2013). Substorm onset and expansion phase intensification precursors seen in polar cap patches and arcs. *Journal of Geophysical Research: Space Physics*, *118*, 2034–2042. https://doi.org/10.1002/jgra.50279

Nishimura, Y., Lyons, L. R., Zou, Y., Oksavik, K., Moen, J. I., Clausen, L. B., et al. (2014). Day-night coupling by a localized flow channel visualized by polar cap patch propagation. *Geophysical Research Letters*, *41*, 3701–3709. https://doi.org/10.1002/2014GL060301

Oksavik, K., Moen, J., & Carlson, H. (2004). High-resolution observations of the small-scale flow pattern associated with a poleward moving auroral form in the cusp. *Geophysical Research Letters*, *31*, L11807. https://doi.org/10.1029/2004GL019838

Oksavik, K., Moen, J., Carlson, H., Greenwald, R., Milan, S., Lester, M., et al. (2005). Multi-instrument mapping of the small-scale flow dynamics related to a cusp auroral transient. *Annales Geophysicae*, *23*(7), 2657–2670. https://doi.org/10.5194/angeo-23-2657-2005

Paschmann, G., Quinn, J., Torbert, R., Vaith, H., McIlwain, C., Haerendel, G., et al. (2001). The Electron Drift Instrument on Cluster: Overview of first results. *Annales Geophysicae*, *19*(10/12), 1273–1288. https://doi.org/10.5194/angeo-19-1273-2001

Pedersen, A., Lybekk, B., André, M., Eriksson, A., Masson, A., Mozer, F., et al. (2008). Electron density estimations derived from spacecraft potential measurements on cluster in tenuous plasma regions. *Journal of Geophysical Research*, *113*, A07S33. https://doi.org/10.1029/2007JA012636

Prikryl, P., MacDougall, J. W., Grant, I. F., Steele, D. P., Sofko, G. J., & Greenwald, R. A. (1999). Observations of polar patches generated by solar wind Alfvén wave coupling to the dayside magnetosphere. *Annales Geophysicae*, *17*(4), 463–489. https://doi.org/10.1007/s00585-999-0463-0

Reiff, P. H., & Burch, J. (1985). IMF By-dependent plasma flow and Birkeland currents in the dayside magnetosphere: 2. A global model for northward and southward IMF. *Journal of Geophysical Research*, *90*(A2), 1595–1609. https://doi.org/10.1029/JA090iA02p01595

Reme, H., Aoustin, C., Bosqued, J., Dandouras, I., Lavraud, B., Sauvaud, J., et al. (2001). First multispacecraft ion measurements in and near the Earth's magnetosphere with the identical Cluster Ion Spectrometry (CIS) experiment. *Annales Geophysicae*, *19*(10/12), 1303–1354. https://doi.org/10.5194/angeo-19-1303-2001

Ruohoniemi, J., & Greenwald, R. (1996). Statistical patterns of high-latitude convection obtained from Goose Bay HF radar observations. *Journal of Geophysical Research*, *101*(A10), 21,743–21,763. https://doi.org/10.1029/96JA01584

Sandholt, P., Farrugia, C., Denig, W., Cowley, S., & Lester, M. (2003). Spontaneous and driven cusp dynamics: Optical aurora, particle precipitation, and plasma convection. *Planetary and Space Science*, *51*(12), 797–812. https://doi.org/10.1016/S0032-0633(03)00114-4

Schunk, R., & Nagy, A. (2009). *Ionospheres: Physics, Plasma Physics, and Chemistry*. Cambridge: Cambridge University press.

Shiokawa, K., Katoh, Y., Satoh, M., Ejiri, M., Ogawa, T., Nakamura, T., et al. (1999). Development of optical mesosphere thermosphere imagers (OMTI). *Earth, Planets and Space*, *51*(7-8), 887–896. https://doi.org/10.1186/2FBF03353247

Shiokawa, K., Otsuka, Y., & Ogawa, T. (2009). Propagation characteristics of nighttime mesospheric and thermospheric waves observed by optical mesosphere thermosphere imagers at middle and low latitudes. *Earth, Planets and Space*, *61*(4), 479–491. https://doi.org/10.1186/BF03353165

Shiokawa, K., Yumoto, K., Nishitani, N., Hayashi, K., Oguti, T., McEwen, D. J., et al. (1996). Quasi-periodic poleward motions of Sun-aligned auroral arcs in the high-latitude morning sector: A case study. *Journal of Geophysical Research*, *101*(A9), 19,789–19,800. https://doi.org/10.1029/96JA01202

Szita, S., Fazakerley, A., Carter, P., James, A., Travnicek, P., Watson, G., et al. (2001). Cluster PEACE observations of electrons of spacecraft origin. *Annales Geophysicae*, *19*(10/12), 1721–1730. https://doi.org/10.5194/angeo-19-1721-2001

Tsyganenko, N. (1989). A magnetospheric magnetic field model with a warped tail current sheet. *Planetary and Space Science*, *37*(1), 5–20. https://doi.org/10.1016/0032-0633(89)90066-4

Tsyganenko, N. (1995). Modeling the Earth's magnetospheric magnetic field confined within a realistic magnetopause. *Journal of Geophysical Research*, *100*(A4), 5599–5612. https://doi.org/10.1029/94JA03193

Tsyganenko, N. (2002a). A model of the near magnetosphere with a dawn-dusk asymmetry 1. Mathematical structure. *Journal of Geophysical Research*, *107*(A8), 1179. https://doi.org/10.1029/2001JA000219

Tsyganenko, N. (2002b). A model of the near magnetosphere with a dawn-dusk asymmetry 2. Parameterization and fitting to observations. *Journal of Geophysical Research*, *107*(A8), 1176. https://doi.org/10.1029/2001JA000220

Tsyganenko, N., & Sitnov, M. I. (2007). Magnetospheric configurations from a high-resolution data-based magnetic field model. *Journal of Geophysical Research*, *112*, A06225. https://doi.org/10.1029/2007JA012260

Vaith, H., Paschmann, G., Quinn, J., Förster, M., Georgescu, E., Haaland, S., et al. (2004). Plasma convection across the polar cap, plasma mantle and cusp: Cluster EDI observations. *Annales Geophysicae*, *22*(7), 2451–2461. https://doi.org/10.5194/angeo-22-2451-2004

Walker, I., Moen, J., Kersley, L., & Lorentzen, D. (1999). On the possible role of cusp/cleft precipitation in the formation of polar-cap patches. *Annales Geophysicae*, *17*(10), 1298–1305. https://doi.org/10.1007/s00585-999-1298-4

Weber, E. J., Buchau, J., Moore, J., Sharber, J., Livingston, R., Winningham, J. D., & Reinisch, B. (1984). F layer ionization patches in the polar cap. *Journal of Geophysical Research*, *89*(A3), 1683–1694. https://doi.org/10.1029/JA089iA03p01683

Weimer, D. (1995). Models of high-latitude electric potentials derived with a least error fit of spherical harmonic coefficients. *Journal of Geophysical Research*, *100*(A10), 19,595–19,607. https://doi.org/10.1029/95JA01755

Wild, J., Cowley, S. W. H., Davies, J., Khan, H., Lester, M., Milan, S., et al. (2001). First simultaneous observations of flux transfer events at the high-latitude magnetopause by the Cluster spacecraft and pulsed radar signatures in the conjugate ionosphere by the CUTLASS and EISCAT radars. *Annales Geophysicae*, *19*(10/12), 1491–1508. https://doi.org/10.5194/angeo-19-1491-2001

Winningham, J., & Heikkila, W. (1974). Polar cap auroral electron fluxes observed with ISIS 1. *Journal of Geophysical Research*, *79*(7), 949–957. https://doi.org/10.1029/JA079i007p00949

Zhang, Q.-H., Ma, Y.-Z., Jayachandran, P., Moen, J., Lockwood, M., Zhang, Y.-L., et al. (2017). Polar cap hot patches: Enhanced density structures different from the classical patches in the ionosphere. *Geophysical Research Letters*, *44*, 8159–8167. https://doi.org/10.1002/2017GL073439

Zou, Y., Nishimura, Y., Burchill, J. K., Knudsen, D. J., Lyons, L. R., Shiokawa, K., et al. (2016). Localized field-aligned currents in the polar cap associated with airglow patches. *Journal of Geophysical Research: Space Physics*, *121*, 10,172–10,189. https://doi.org/10.1002/2016JA022665

Zou, Y., Nishimura, Y., Lyons, L., Conde, M., Varney, R., Angelopoulos, V., & Mende, S. (2018). Mesoscale F region neutral winds associated with quasi-steady and transient nightside auroral forms. *Journal of Geophysical Research: Space Physics*, *123*, 7968–7984. https://doi.org/10.1029/2018JA025457

Zou, Y., Nishimura, Y., Lyons, L. R., & Shiokawa, K. (2017). Localized polar cap precipitation in association with nonstorm time airglow patches. *Geophysical Research Letters*, *44*, 609–617. https://doi.org/10.1002/2016GL071168

Zou, Y., Nishimura, Y., Lyons, L. R., Shiokawa, K., Donovan, E. F., Ruohoniemi, J. M., et al. (2015). Localized polar cap flow enhancement tracing using airglow patches: Statistical properties, IMF dependence, and contribution to polar cap convection. *Journal of Geophysical Research: Space Physics*, *120*, 4064–4078. https://doi.org/10.1002/2014JA020946